Luminescence spectroscopy of atomic zinc in solid rare gases. II. Temperature dependence

Veronica A. Bracken and Paul N. Kerins
Department of Chemistry, National University of Ireland, Maynooth, County Kildare, Ireland

Peter Gürtler
HASYLAB at DESY, Notkestrasse 85, 22603 Hamburg, Germany

John G. McCaffrey[a)]
Department of Chemistry, National University of Ireland, Maynooth, County Kildare, Ireland

(Received 31 March 1997; accepted 7 July 1997)

The temperature dependence of the pairs of emission bands present for atomic zinc isolated in annealed solid argon, krypton, and xenon samples is examined in steady-state and time-resolved luminescence spectroscopy. The pairs of emission bands in all the Zn/RG systems exhibited a reversible temperature dependence whereby the intensity of the high-energy band decreased, while the low-energy band gained in intensity with increasing temperature. In the Zn/Ar system, the decrease in the intensity of the 218.9 nm emission band observed between 9 and 28 K was coupled with a concomitant increase in the intensity of the band at 238 nm. In this temperature range the decay times of the 218.9 nm band decreased while the 238 nm band exhibited a constant decay time of 1.41 ns and a rise time correlated with the decay of the 218.9 nm band. The interdependence exhibited by the intensities and decay times of the two emission bands is modeled by an activated nonradiative process with a barrier height of 130.6 cm^{-1} for population interconversion between the pairs of emitting levels on of the spin singlet adiabatic potential energy surface. Similar behavior was observed in Zn/Kr between 6.3 to 20 K, but at higher temperatures this system also exhibited enhanced intersystem crossing. Likewise, for Zn/Xe, the low-energy 399 nm emission increased in intensity at the expense of the high-energy 356 nm emission up to a temperature of 40 K. For the Zn/Kr pair of singlet emissions and the Zn/Xe pair of triplet emissions, barrier heights of 78.1 and 42.6 cm^{-1} were evaluated, respectively. © *1997 American Institute of Physics.*
[S0021-9606(97)00738-1]

I. INTRODUCTION

In this paper the temperature dependence of the pairs of emission bands present for atomic zinc isolated in annealed solid argon, krypton, and xenon matrices (Zn/RG) is examined in steady-state and time-resolved measurements. The low-temperature luminescence spectroscopy of atomic zinc isolated in these solids has been presented in the preceding paper,[1] which will be referred to hereafter as Paper I. A summary of the spectra recorded for the Zn/RG systems is given in Fig. 6 of Paper I. Based on their spectral positions and temporal characteristics, the pairs of emission bands present in the uv spectral region for Zn/Ar and Zn/Kr were assigned in Paper I to the singlet $4p\ ^1P_1 \rightarrow 4s\ ^1S_0$ transition of atomic zinc, while the exclusive near-uv pair of Zn/Xe and the single near-UV emission of Zn/Kr were assigned to the triplet $4p\ ^3P_1 \rightarrow 4s\ ^1S_0$ transition. The threefold splitting of the excitation profiles was ascribed to the dynamic Jahn-Teller effect in a previous absorption study.[2] The origin of the pairs of emission bands was identified in a recent theoretical study[3] to the coexistence of two nondegenerate minima on the same adiabatic potential energy surface (APES) as a consequence of dynamic Jahn-Teller coupling in the excited $4s4p\ ^1P_1$ state of atomic zinc.

The observation of pairs of emission bands, both assigned to the same electronic transition, is the first of its kind to be reported for the luminescence of a degenerate excited state of a metal atom isolated in solid rare gases. It should be pointed out that the atomic emission of the matrix-isolated alkali[4] and coinage[5] group metal atoms frequently exhibit pairs of emission bands. However, the excited spin doublet *P* terms in these systems are already split because of spin–orbit coupling rendering an unambiguous identification of the nature of the splitting impossible. To investigate further the origin of the emission pairs in the simpler Zn/RG systems, the temperature dependence of the luminescence is now examined with steady-state and time-resolved measurements.

II. EXPERIMENT

Optical measurements were conducted at the HIGITI experimental station in HASYLAB at DESY, Hamburg using synchrotron radiation. A detailed description of the experimental setup has been presented in Paper I,[1] so only a brief outline will be given here. Solid samples were prepared[6] at cryogenic temperatures by the cocondensation of atomic zinc metal vapor, produced from a 1 mm diameter zinc rod with an Omicron EFM3 UHV evaporator, and the rare gases Ar, Kr, and Xe. All the samples used in the present study were annealed,[6] as described in Paper I, prior to the recording of

a)Author to whom correspondence should be addressed.

 0021-9606/97/107(14)/5300/10/$10.00

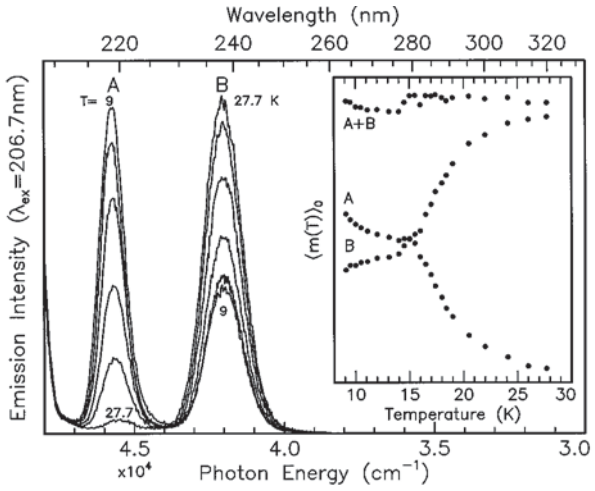

FIG. 1. Temperature dependence of the intensities of the *A* and *B* emission bands, centered at 218.9 and 238 nm, respectively, in the Zn/Ar system. The emission spectra shown were recorded using a fixed excitation wavelength of 206.7 nm at temperatures of 9, 11, 16, 18, 20, and 27.7 K. The inset displays the relationship between the integrated intensities of the *A* and *B* emission bands as well as their sum $(A+B)$ as a function of temperature. The intensities were evaluated from the zeroth moment of the emission bands.

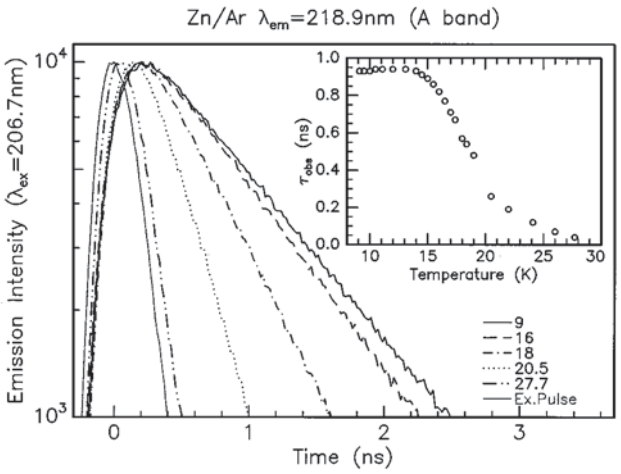

FIG. 2. Decay profiles recorded, as a result of 206.7 nm excitation, for the *A* (218.9 nm) emission band of Zn/Ar at the indicated temperatures. Only the portions at maximum intensity in the decay profiles are shown to illustrate the differences existing at the specified temperatures. The inset displays the observed decay times, extracted over the entire decay curves, for all measurements made as a function of temperature.

any data. Steady-state luminescence measurements were made with either a 0.4 m Seya–Namioka monochromator for the VUV and near-UV regions or a 0.2 m Acton Research Corporation Type VM 502 monochromator for the uv-visible region. Nanosecond lifetime measurements of the emission bands in the Zn/RG systems were made using the time correlated single photon counting (TCSPC) technique.[7] The associated decay times were extracted using the ZFIT program[8] by fitting trial functions, convoluted with the temporal profile of the excitation pulse, to the recorded decay curves.

III. RESULTS

A. Zn/Ar Jahn-Teller interconversion

A reversible temperature dependence was observed in annealed Zn/Ar samples for the pair of spin singlet $^1T_{1u} \rightarrow {}^1A_{1g}$ emission bands whereby the intensity of the low-energy emission band at 238 nm, labeled *B*, increased with increasing temperature at the expense of the high-energy *A* emission band at 218.9 nm. The spectra and integrated intensities of the Zn/Ar *A* and *B* emission bands, recorded for specific temperatures in the range 9–27.7 K using a fixed photoexcitation wavelength of 206.7 nm, are shown in Fig. 1. The inset in Fig. 1 is a plot of the integrated intensities of the pair of emission bands, calculated from the zeroth moment[9] of the band profiles which demonstrates quantitatively, that the decrease in the intensity of the *A* band corresponds to the increase in the intensity of the *B* band. From the constant behavior exhibited by the sum of the intensities of the two emission bands $(A+B)$ in Fig. 1, it is concluded that the quantum yield for singlet emission in the Zn/Ar system remains constant in the temperature range studied. However, from the form of the integrated intensities shown in the inset of Fig. 1 for the *A* and *B* emission bands, it is evident that two distinct temperature dependences exist in the Zn/Ar system. Thus at lower temperatures the change in the intensity is initially gradual, becoming more pronounced above 14 K.

Decay profiles recorded for the Zn/Ar high-energy *A* emission band with excitation at 206.7 nm using the TCSPC technique, also showed a pronounced temperature dependence as shown in Fig. 2. The inset of Fig. 2 indicates that the observed decay times[10] of this band are independent of temperature up to 13 K, having a value of 0.93 ns, but for higher temperatures the decay times becomes shorter. The decay time found to be independent of temperature, i.e., $\tau = 0.93$ ns for $T < 13$ K is taken, as quoted in Paper I, to be the radiative lifetime of the 218.9 nm emission band.

In contrast to the decay profile of the *A* emission, which exhibits a dominant single decay time component, a rise time and a constant decay time of 1.41 ns were present in the decay profiles of the *B* emission band at 238 nm. Four decay curves recorded at the indicated temperatures for the *B* band, are shown in Fig. 3. The entire decay curve consists of two components, both with a decay time of 1.41 ns, one with an instantaneous rise time, the other detectable with the 100 ps temporal resolution of the present apparatus. At the lowest temperature of 9 K, the presence of the rise-time component is clearly evident from the bulge of the recorded decay profile. In the temperature range 9–13.1 K, evidence of this rise-time component becomes less obvious, while at higher temperatures its contribution once more becomes most significant at 18 K. At temperatures greater than 18 K the rise-time component is getting shorter and its contribution to the shape of the decay profile is diminishing. Hence extraction of the rise time in the fitting procedure is more prone to error at these higher temperatures. The inset of Fig. 3 shows the temperature dependence of the recorded decay and observed

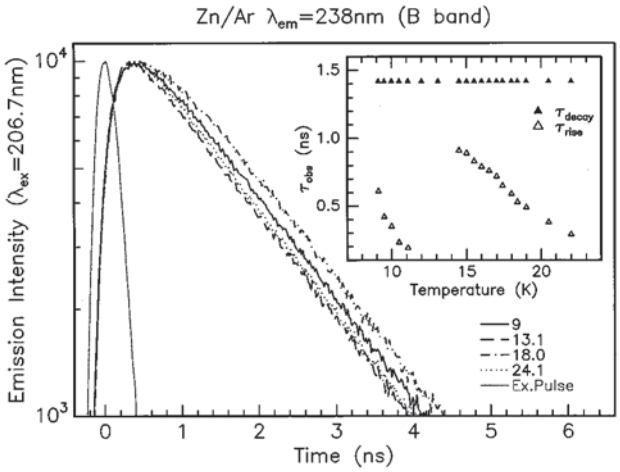

FIG. 3. Decay curves of the Zn/Ar *B* (238 nm) emission band recorded at the temperatures specified by the legend. The inset shows the temperature dependence of the decay and rise time present in the decay profile of the *B* band. The decay component has a value of 1.41 ns and is independent of temperature. The rise time is present in two temperature regimes, i.e., up to 11 K and above 14 K, and strongly temperature dependent in both.

rise times of the *B* emission band. It can be seen that the former is independent of temperature, while the latter is present in two temperature regimes, viz., up to 11 K and beyond 14 K and strongly temperature dependent in both. In the left panel of Fig. 4, the observed decay times of the *A* band, shown already in Fig. 2, and rise times of the *B* band (Fig. 3) are shown together as a function of temperature in the range 9–29 K. It is clearly evident in this figure that a strong correlation exists between the pair of data sets above 14 K.

The decrease in the intensity of the Zn/Ar high-energy *A* emission band with increasing temperatures and the increase

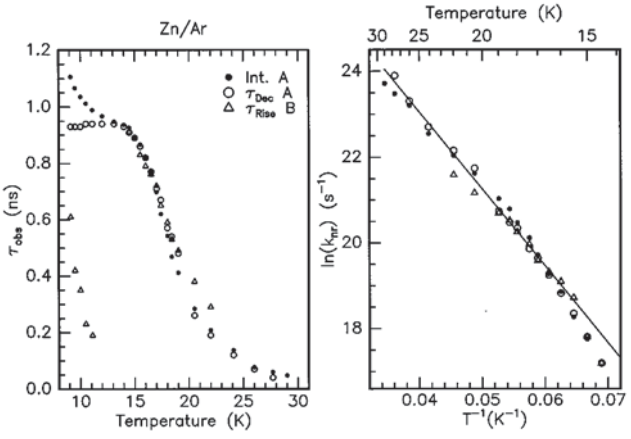

FIG. 4. The panel on the left shows the temperature dependence of the observed decay times of the *A* band measured directly and from the intensity measurements, as well as the observed rise time in the *B* level. Note the strong correlation existing between all three data sets for temperatures greater than approximately 13 K. The panel on the right is an Arrhenius plot showing the nonradiative rate constants, $k_{\rm nr}$, extracted from the observed lifetimes, $\tau_{\rm obs}$, presented on the left, in the temperature regime in which a correlation exists between the three data sets.

in the intensity of the low-energy *B* emission band at 238 nm shown in Fig. 1 is fully reversible. That is, the original low-temperature spectra can be regenerated exactly after going through the heating cycle. This reversible behavior of the intensities when taken in conjunction with the strong correlation existing between the rise times of the *B* emission band and the decay times of the *A* band, indicates that the high-energy *A* (218.9 nm) level feeds the low-energy *B* (238 nm) in the higher-temperatures regime, i.e., greater than 14 K. Furthermore, considering that the overall singlet state emission quantum yield in the Zn/Ar system remains constant in the heating cycle, as indicated by the $A+B$ integrated intensities shown in the inset in Fig. 1, only a single temperature-dependent nonradiative process connects the two emission bands, without competition of a nonradiative step leading to the ground state. To examine the underlying nonradiative process some photophysical relations will now be presented.

The relationship between the observed decay rate constant $k_{\rm obs}$ and the radiative decay k_r of the high-energy 218.9 nm emission is given by the following equation

$$k_{\rm obs}=k_r+k_{\rm nr}. \tag{1}$$

It is assumed in Eq. (1), for the reasons presented in the preceding paragraph, that only a single nonradiative process, with a rate constant $k_{\rm nr}$, is responsible for the depopulation of the emitting *A* level. Equation (1) can also be expressed as

$$1/\tau_{\rm obs}=1/\tau_r+1/\tau_{\rm nr} \tag{2}$$

in terms of time constants or observed lifetimes, $\tau_{\rm obs}$. The intensity of the high-energy *A* emission band at any temperature, T, is related to its observed decay rate constant $k_{\rm obs}$ at this particular temperature as

$$\frac{I_T}{I_0}=\frac{k_r}{k_{\rm obs}}, \tag{3}$$

where I_T and I_0 are the intensities of the *A* band in the presence and absence of the nonradiative process, respectively. Rearranging Eq. (3) and expressing as an observed lifetime we obtain

$$\tau_{\rm obs}=\tau_r\,\frac{I_T}{I_0}, \tag{4}$$

an expression which allows the decay time of the *A* band to also be extracted from emission intensity measurements once the radiative lifetime τ_r of this emission is known.

The radiative decay time τ_r of the 218.9 nm band was identified as 0.93 ns in the low-temperature regime ($T<13$ K) in which no variation exists in the observed decay, as shown by the inset of Fig. 2. The value for I_0 to be used in Eq. (4) was selected[11] as the intensity recorded at 13 K, since (a) the decay time of the *A* level showed no variation up to this temperature and (b) this is the onset of the strong second temperature dependence exhibited in the Zn/Ar intensity measurements as shown in Fig. 1. A comparison of all the observed Zn/Ar lifetime data is made on the left in Fig. 4 where the intensities and the directly measured decay times of the *A* band are shown together as a function of temperature, as well as the rise times of the *B* band.

Clearly there is a correlation between the observed decay times of the 218.9 nm emission and the observed rise times of the 238 nm band. The significance of this correlation can be identified from the integrated rate expressions given by Eqs. (A10) and (A11) in the Appendix for the two emitting levels of a four-level, five-step scheme considered. These rate expressions pertain to a relaxation mechanism in which a *single* nonradiative process, having a rate constant k_{nr}, connects the higher and lower energy emitting levels. For such a mechanism, Eq. (A11) indicates that the rise time of the lower-energy B level is *identical* to the observed decay of the higher-energy A level, Eq. (A10). The agreement existing between the observed decay time of the 218.9 nm emission and the rise time of the 238 nm emission demonstrates that this is the case for the Zn/Ar system for temperatures greater than 14 K. Furthermore, given the good agreement found between the intensity and the decay time data, it can be concluded that this single nonradiative step is the only one depleting the A level. This last point is consistent with the conclusions drawn already from the temperature invariance exhibited in the spin singlet emission quantum yield.

In the low-temperature regime, $T<13$ K, the shortening of the rise time on the B band appears to track the decreasing intensity of the A band as shown in Fig. 4. However, given the invariance of the A band emission decay times for temperatures up to 13 K, one must conclude, from the kinetic expressions (A5) and (A7) given in the Appendix, that the temperature dependence of the intensities of the A and B emission bands in this lower temperature range is due to changes in the relative rates, i.e., branching ratios, of the two competing steps k_1 and k_2 populating the A and B emitting levels immediately after optical excitation.

Rewriting[12,13] Eq. (2) in terms of the nonradiative rate k_{nr},

$$k_{\mathrm{nr}}=1/\tau_{\mathrm{obs}}-1/\tau_r \tag{5}$$

allows extraction of this quantity from the observed lifetime data shown in the left panel of Fig. 4 since the radiative lifetime τ_r of the A band is known to be 0.93 ns. A plot of $\ln(k_{\mathrm{nr}})$ is made against reciprocal temperature in the right panel of Fig. 4 for the regime ($T>13$ K) in which a correlation was observed to exist between all the observed decay times for the 218.9 nm band and the rise times of the 238 nm band. A plot of the values of $\ln(k_{\mathrm{nr}})$ extracted from the observed rise time of the 238 nm emission against $1/T$ is shown by the triangles in Fig. 4.

The linear behavior observed in Fig. 4 for *all three* $\ln(k_{\mathrm{nr}})$ data sets indicates that the nonradiative process of interconversion between the A and B emitting levels can be described by the Arrhenius equation. In this equation the temperature dependence of the nonradiative rate constant k_{nr} is given by

$$k_{\mathrm{nr}}=A\ \exp\left(\frac{-E_{\mathrm{act}}}{kT}\right), \tag{6}$$

in which k is Boltzmann's constant and T is the temperature. The activation energy E_{act} and the pre-exponential factor A were determined from the slope and the intercept of the fit of the data as 130.6 cm^{-1} and 2.07×10^{13} s^{-1}, respectively. E_{act} is the barrier height encountered on going from the higher-energy emitting level A to the lower-energy emitting level on the same APES as shown by the schematic diagram in Fig. 9 of Paper I. In this model, tunneling through the barrier has been neglected, thus the activation energy extracted should be considered as an effective value.

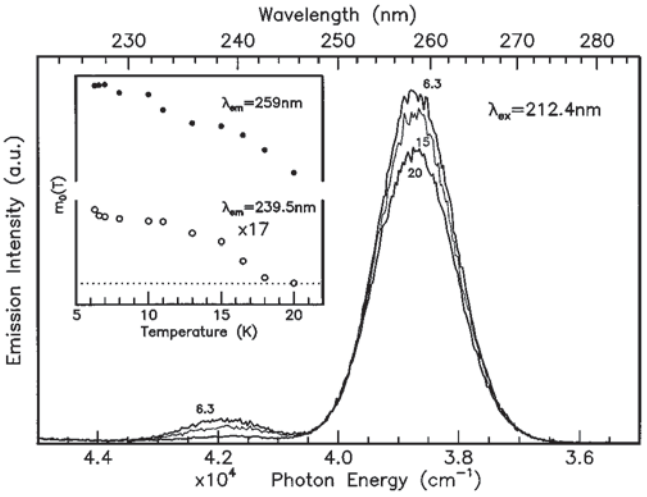

FIG. 5. Temperature dependence of the emission intensities of the Zn/Kr bands centered at 239.5 and 259 nm. A fixed photoexcitation wavelength of 212.4 nm was used for all the spectra recorded in the temperature range indicated in the figure. The inset displays the behavior of the integrated intensities of the two emission bands as a function of temperature. The horizontal dotted line indicates the zero intensity of the 239.5 nm emission band.

B. Zn/Kr Jahn-Teller interconversion

In this section the temperature dependence of the pair of singlet emission bands at 239.5 and 259 nm in Zn/Kr will be presented. In contrast to the Zn/Ar system, an additional channel, however, exists in Zn/Kr which is especially important at higher temperatures for relaxation of the singlet state population. Specifically, a strongly temperature dependent intersystem crossing (ISC) occurs between the excited singlet state and the metastable triplet states in addition to the interconversion of the spin singlet emission bands. For temperatures less than 10 K only a slight variation exists in the intensities of the 239.5 nm emission band as shown by the integrated intensities (zeroth moment) in the inset on the left in Fig. 5, while above 10 K a pronounced drop is observed. Although the intensity of the 239.5 nm emission is decreasing above 10 K, a corresponding increase of the 259 nm emission is not observed due to ISC from the singlet surface to the triplet surface. The effect of ISC on Zn/Kr luminescence will be addressed later in this paper.

The decay profiles recorded for the 239.5 nm emission band at specific temperatures, all produced with photoexcitation at 212.4 nm, are shown in the panel on the left in Fig. 6. The decay profiles were fitted using two exponential functions of which the major decay component, having a magnitude of 1.26 ns at low temperatures ($T=6$ K) and contributing to over 93% of the decay profile, was taken as the

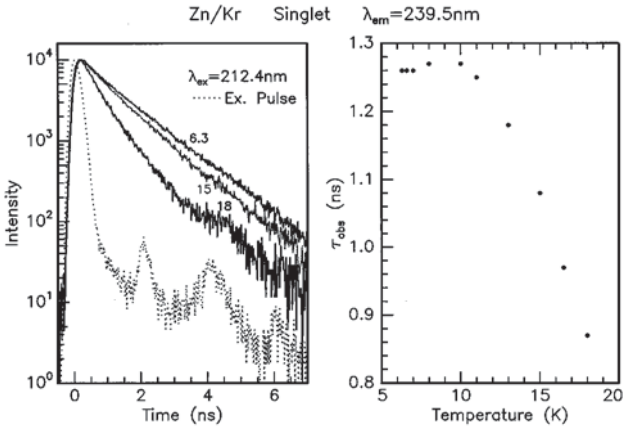

FIG. 6. Temperature dependence of the decay profiles of the Zn/Kr 239.5 nm emission band. All the decay profiles were recorded with pulsed excitation at 212.4 nm. The decay times observed in the measurements made in the temperature range 6–18 K are shown in the panel on the right.

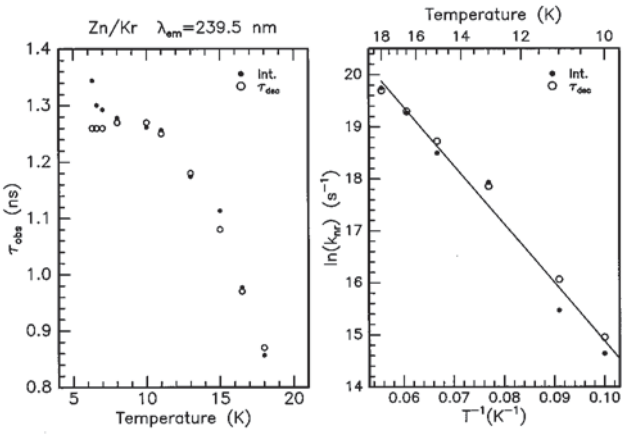

FIG. 8. An Arrhenius plot of the activated process coupling the Jahn-Teller minima of the Zn/Kr system. The panel on the left shows the decay times of the 239 nm emission band observed directly in lifetime measurements and extracted indirectly from intensity data. The panel on the right shows an Arrhenius plot of the nonradiative rate constants extracted from all the lifetime data observed above 10 K.

observed decay time of the 239.5 nm emission band. The observed decay times shown in the panel on the right in Fig. 6 demonstrate that the lifetime of the 239.5 nm emission band is independent of temperatures up to 10 K, exhibiting a pronounced shortening above this value.

A different temperature dependence has been identified in the recorded decay profiles of the 259 nm emission band. Evidence of a rise time and a constant decay time of 1.60 ns were detected for temperatures up to 9 K. In Fig. 7, decay profiles recorded at the indicated temperatures for the 259 nm emission band are presented. The panel on the right in Fig. 7 shows the decay times and the rise times extracted from all the 259 nm decay profiles measured between 6 and 42 K.

As in the emission of the Zn/Ar system, the model of two nondegenerate minima separated by an activation energy barrier will be used to account for the reversible behavior exhibited by the pair of spin singlet emission in the Zn/Kr system. The radiative decay of the 239.5 nm emission band was identified as 1.26 ns from the invariance of its observed decay times in the low-temperature regime 6.3 to 10 K. The directly observed lifetimes of the 239.5 nm band obtained from the recorded decay curves and the τ_{obs} values extracted from the intensity data of this band, using the previously identified radiative lifetime of 1.26 ns in Eq. (4), are shown on the left in Fig. 8. The intensity of the 239.5 nm band at 10 K was chosen as the value for I_0 as this was the temperature, as shown in Fig. 8, at which the observed lifetime of the emission became temperature dependent. The nonradiative contributions to the observed lifetimes extracted from the decay curves and intensity data are represented by closed and open circles, respectively, in the Arrhenius plot presented on the right in Fig. 8. Accordingly an activation energy of 78.1 cm^{-1} and an Arrhenius frequency factor of 2.20 $\times 10^{11}$ s^{-1} were extracted from the slope and intercept, respectively, of the linear fit shown.

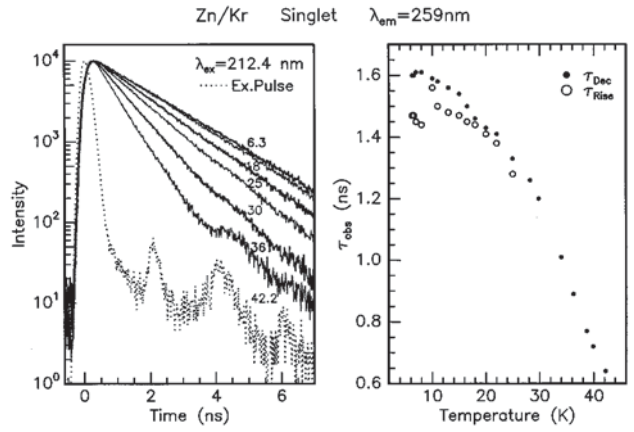

FIG. 7. Temperature dependence of the 259 nm emission decay profiles in the Zn/Kr system at the specified temperatures. The time structure of the synchrotron excitation pulse is represented by the dotted trace. In the panel on the right the extracted decay and rise times in the 259 nm emission band are shown for all measurements made up to 42 K.

As observed in the Zn/Ar system, the intensity of the high-energy band in Zn/Kr exhibits a temperature dependence even though its decay times show no variation for temperatures less than 10 K. Such behavior is ascribed to the temperature-dependent branching ratio feeding emitting levels immediately after excitation of the ^1P level at 212.4 nm. Thus the rise times observed for the 259 nm emission band at temperatures lower than 10 K are a consequence of slow relaxation occurring after branching of the optical excitation has occurred. For temperatures above 10 K, two rise-time components are therefore expected, one is associated with slow relaxation occurring immediately after absorption, the other is associated with the onset of the activated Jahn-Teller interconversion process. However, only a single effective rise time was extracted from the decay curves for temperatures above 10 K. Because of this complication, the extracted rise times have not been used in the Zn/Kr system as another means of determining the activation energy barrier, as they were in the Zn/Ar system.

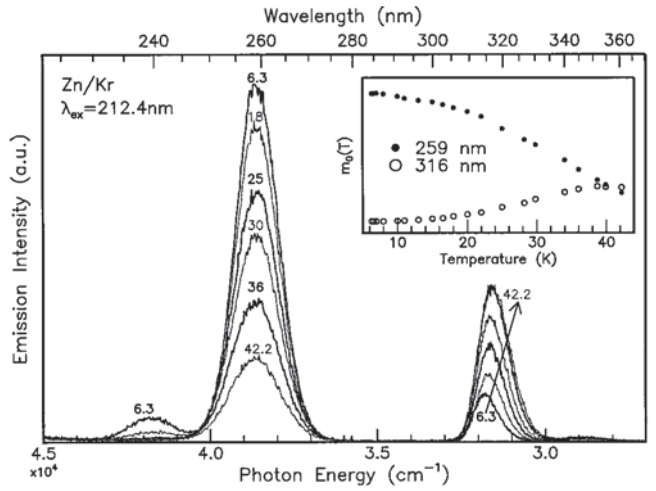

FIG. 9. Temperature dependence of the intensities of the singlet and the triplet emission bands in the Zn/Kr system. All emission spectra were recorded using a fixed excitation wavelength of 212.4 nm. The inset on the top right is a plot of the integrated emission intensities of the singlet 259 nm and the triplet 316 nm emission bands recorded as a function of temperature.

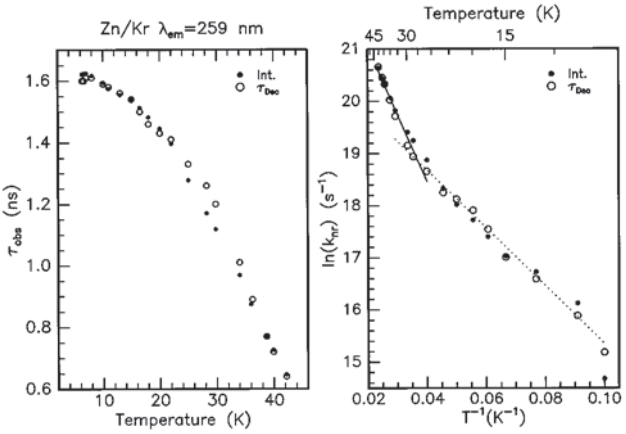

FIG. 10. A plot of the temperature dependence of the decay time of the 259 nm emission band in the Zn/Kr system as observed directly in decay profiles and extracted from intensity measurements. The panel on the right shows an Arrhenius plot of the nonradiative rate constants extracted from the observed decay times shown on the left using a radiative lifetime of 1.62 nm for the 259 nm emission. Two linear portions clearly exist, one for the temperatures below 28 K and the other for temperatures above 28 K as indicated by the dotted and solid lines, respectively.

C. Zn/Kr intersystem crossing

In addition to the pair of spin singlet emission bands present in the uv spectral region, photoexcitation of the singlet absorption of Zn/Kr at 212.4 nm produces a single emission band in the near-uv region, assigned in Paper I to the triplet emission. Identical excitation spectra were recorded, as reported in Paper I, by monitoring either of the pair of singlet emissions or the triplet emission.[1] Thus it is inferred that optical pumping of the singlet transition results in population of the $^3T_{1u}$ state via nonradiative decay of the $^1T_{1u}$ state. This intersystem crossing (ISC) in Zn/Kr exhibits the temperature dependence shown in Fig. 9, whereby the intensity of the triplet emission band increases at the expense of the singlet emission intensity with increasing temperature. Plots of the integrated intensities (zeroth moment) of the singlet 259 nm emission band and the triplet 315.6 nm emission band are indicated by the filled and open circles, respectively, in the inset of Fig. 9. Up to a temperature of 7 K the intensity of both the singlet 259 nm emission and the triplet 315.6 nm emission are constant, indicating that the onset of ISC occurs at a temperature greater than this, identified tentatively as 8 K.

As discussed earlier, decay curves recorded at specific temperatures for the 259 nm emission band showed a pronounced temperature dependence. The shortening of the observed decay times of the 259 nm emission band as a function of increasing temperature is shown on the right side of Fig. 7 in the range 6–42 K.

Steady-state and time-resolved data of the 259 nm singlet emission band were treated in a fashion similar to that described earlier in the temperature dependence of the Zn/Ar or Zn/Kr singlet emission bands, in order to determine the activation energy barrier of the ISC process in Zn/Kr. The value of I_0 in Eq. (5) was selected as the intensity of the 259 nm at 7 K because ISC is present for all temperatures greater than this. A plot of the k_{nr} values obtained with Eq. (5) from decay time measurements [Eq. (2)] and from intensity data [Eq. (4)] of the 259 nm band are shown on a logarithmic scale versus inverse temperature in Fig. 10. The activation energy barrier and Arrhenius frequency factor extracted for the ISC process from the fit are 38.6 cm^{-1} and 1.20×10^9 s^{-1}, respectively, in the temperature range 10 to 28 K. For temperatures above 28 K another linear region exists in the Arrhenius plot shown in Fig. 10 having an activation energy of 95.6 cm^{-1} and a frequency of 2.32×10^{10} s^{-1}. It is noteworthy in Fig. 9 that in the higher temperature regime, i.e., above 28 K, the decrease in the intensity of the 259 nm emission band is not accompanied by a corresponding increase in the intensity of the triplet emission band. This behavior indicates that some other nonradiative process must be competing with ISC for decay of the excited singlet state population. Given the sparsity of the energy levels of atomic zinc in this spectral region the only other process possible is one which couples the excited singlet state directly to the singlet ground state, a process referred to as internal conversion (IC) in the photophysics literature of organic molecules.

D. Zn/Xe Jahn-Teller interconversion

The intensities of the triplet emission bands of Zn/Xe at 356 and 399 nm exhibited the temperature dependence shown in the panel on the left side of Fig. 11. The integrated intensities of the emission bands, shown on the right side of Fig. 11, quantitatively demonstrate that the intensity of the high-energy band at 356 nm decreases promptly from 9 K coupled with a concomitant increase of the low-energy emission band centered at 399 nm as the temperature is increased. Since the decay times of the Zn/Xe near-uv emission bands were too long to be measured at the synchrotron experiment,[14] we cannot, however, demonstrate in the

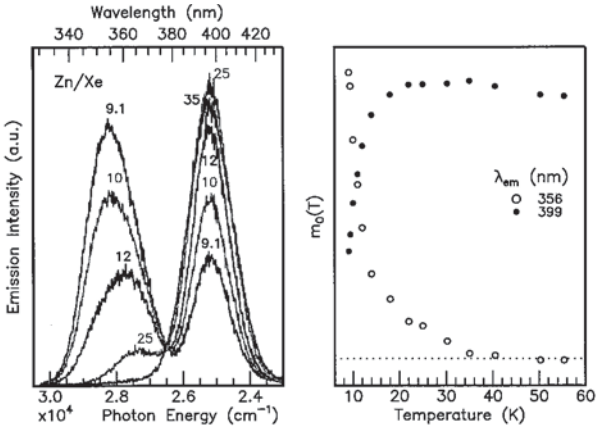

FIG. 11. Temperature dependence of the triplet emission in the Zn/Xe system. The emission spectra shown in the left panel were recorded with a fixed excitation wavelength of 219.9 nm at the specified temperatures. The panel on the right shows a plot of the integrated intensities of the emission bands as a function of temperature, which demonstrates their interdependent relationship. The horizontal dotted line indicates zero intensity of the 356 nm emission band.

present work that the low-energy emitting level at 399 nm is populated exclusively from the high-energy level at 356 nm.

The temperature dependence of the intensity data can nonetheless be used, by plotting $\ln(k_{nr})$ in Eq. (5) versus reciprocal temperature, to evaluate the activation energy barrier in this system. However, even Eq. (5) requires the use of the radiative lifetime of the upper emitting level, which also has not been measured. As an estimate of the radiative lifetime for the Zn/Xe matrix 356 nm emission band, the gas phase value of 30.4 μs was used. Accordingly, from a linear fit[15] of the 356 nm emission intensity data, shown on the right side in Fig. 11, an activation energy barrier of 42.6 cm^{-1} and a frequency factor of 5.17×10^{6} s^{-1} were evaluated. The value of I_0 used was obtained from the lowest measurement temperature of 9 K but it must be conceded, and as highlighted in the Zn/Ar system, that in the absence of time resolved data, the selection of the value of I_0 is arbitrary. Hence considerable uncertainty is associated with the value of 42.6 cm^{-1} obtained for the height of the activation energy barrier in the Zn/Xe system.

IV. DISCUSSION

The Zn/RG system in which the most detailed kinetic study has been conducted and for which the most accurate results have been extracted, is the interconversion between the pair of spin singlet emission bands in the Zn/Ar system. This is the case for the following reasons: (a) the time scale of the decay of the Zn/Ar singlet emission is particularly well matched to the time resolution of the present experimental apparatus and (b) the dynamics on the singlet surface can be investigated in isolation from other temperature dependent processes such as ISC or IC. The latter two processes are observed in the Zn/Kr system, while the operation frequency of the synchrotron radiation is too high for lifetime measurements on the triplet emission of the Zn/Xe system. For these reasons the temperature dependence of the Zn/Ar system will be considered in detail in a forthcoming publication and compared with theoretical predictions[3] of these phenomena derived using potential energy surfaces generated with Zn·Ar and Ar·Ar pair potentials.

TABLE I. Arrhenius parameters and onset temperatures of activated Jahn-Teller processes between the pairs of singlet UV emissions in Zn/Ar, Zn/Kr, and triplet near-uv emission pairs of Zn/Xe. The second to last row of the table pertains to the Arrhenius parameters for $^1T_{1u}\rightarrow{}^3T_{1u}$ intersystem crossing ISC in Zn/Kr, the last row to $^1T_{1u}\rightarrow{}^1A_{1g}$ internal conversion (IC).

Zn/RG	E_{act} (cm^{-1})	A_0 (s^{-1})	Onset temp. (K)
Zn/Ar	130.6	2.07×10^{13}	14
Zn/Kr	78.1	2.20×10^{11}	10
Zn/Xe	42.6	5.17×10^{6} [a]	<9
Zn/Kr (ISC)	38.6	1.20×10^{9}	8
Zn/Kr (IC)	95.6	2.32×10^{10}	28

[a]The Arrhenius frequency factor was evaluated using the gas phase radiative lifetime 30.4 μs of triplet $4p\ ^3P_1\rightarrow4s\ ^1S_0$ transition of atomic zinc.

As noted earlier, the intensity of the triplet emission band in the Zn/Kr system showed no variation for temperatures up to 7 K. In this temperature regime, the intensities and decay times of the 259 nm emission band were constant. An increase in the intensity of the 316 nm emission band was observed only when a decrease in the intensity of the 259 nm band occurred. Inspection of the decay times of the 239.5 nm emission band shown on the left side in Fig. 8 reveal that no variation is observed even up to temperatures of 10 K. From the invariance of the decay times of the 239.5 nm emission band for temperatures higher than those required to produce a change in the intensity of the triplet emission, it is concluded that the 239.5 nm minima does not feed the 316 nm minima of the $^3T_{1u}$ surface via ISC.

Based on the observations presented in the preceding paragraphs, it might appear that the $^3T_{1u}$ surface intersects with the 259 nm minima of the $^1T_{1u}$ surface and not with the 239.5 nm minima on the same APES. However, a comparison of the Arrhenius frequency factors quoted in Table I indicates that such a conclusion is not so definitive. For temperatures lower than 28 K, the Arrhenius frequency factor for Jahn-Teller interconversion listed in Table I is about two orders of magnitude greater than that of ISC which indicates that Jahn-Teller interconversion between the singlet minima is much more efficient than ISC. Given that the Jahn-Teller activated process is more efficient than ISC, the effect of ISC via the 239.5 nm minima is masked to such an extent that it does not manifest itself in the loss of intensity of the 239.5 singlet emission band. Hence one cannot draw the conclusion that the repulsive triplet surface does not cross the singlet surface producing the higher-energy 239.5 nm emission.

V. CONCLUSIONS

The temperature dependence of the steady-state and time-resolved spectroscopy of the pairs of spin singlet uv emission bands in Zn/Ar and Zn/Kr are modeled by an activated nonradiative process coupling the two minima of different symmetry which coexist on the same APES as a result of Jahn-Teller coupling. Their intensities exhibited a revers-

ible temperature dependence whereby the high-energy emission band decreased in intensity coupled with a corresponding increase in the intensity of the low-energy emission. Similar behavior was observed for the near-uv spin triplet emission in Zn/Xe. A summary of the Arrhenius parameters and the onset temperatures of the activated nonradiative process for the Zn/RG systems are shown for the purpose of comparison in Table I.

Having identified the onset temperature of the activated processes in the Zn/Ar and Zn/Kr uv emissions, it was inferred that the variance of the intensity measurements for temperatures lower than the onset temperature was attributed to the relative relaxation rates from the excited surface occurring immediately after ^1P optical excitation. From the observed rise times, a temperature dependent rate determining step (RDS) was identified in the relaxation route populating the 238 nm level of Zn/Ar in the low-temperature regime ($T<13$ K). This step was no longer rate determining for temperatures greater than 11.1 K. Similarly, a temperature dependent RDS was identified in the decay of the low-energy emission 259 nm emission band in Zn/Kr up to a temperature of 10 K. Given the long (ns) rise times present on the low-energy emission bands in Zn/Ar and Zn/Kr it could be proposed that radiative decay of a shallow precursor level is responsible for the observed rise times. A candidate for the emission of such a precursor level might be the higher energy bands present in Zn/Ar and Zn/Kr. However, as indicated in the Appendix if feeding of the low-energy level by the precursor occurs then the decay time of the precursor must be identical to the rise time observed in the low-energy emission bands. This rules out the high-energy bands as candidates since they show decay times different to the rise times on the lower energy emissions.

For higher temperatures, the presence of another rise time in the lower-energy bands emerges as a consequence of the onset of the activated Jahn Teller interconversion process between the emitting levels. As stated in the Discussion, the nature of the activated interconversion process in the Zn/Ar system is currently being examined theoretically[16] with potential energy surfaces generated from Zn·Ar and Ar·Ar pair potentials. Preliminary results, obtained for PES arising from a coupling of the two vibronic modes leading to the pair of emission bands indicate that the activation energy barriers can be predicted with accuracy using pair potentials.

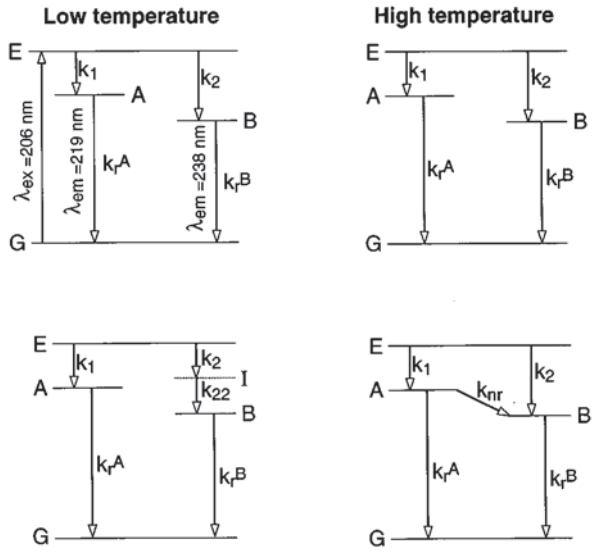

FIG. 12. Relaxation schemes considered to model the kinetics exhibited by the pairs of emission bands in the Zn/RG matrix systems. The wavelengths listed on the top left are particular to the singlet emission pair in the Zn/Ar system.

APPENDIX

1. Low-temperature kinetics

The simplest kinetic scheme which can be presented to model the existence of the pair of emission bands produced from a common excitation is a four level scheme indicated on the top left of Fig. 12. The key assumption in this model is that the steps k_1 and k_2, leading to the populating of levels A and B from the level E reached in absorption, exist in competition. The rate equations for this scheme are

$$\dot{n}_E = -k_1 \cdot n_E - k_2 \cdot n_E, \tag{A1}$$

$$\dot{n}_A = -k_r^A \cdot n_A + k_1 \cdot n_E, \tag{A2}$$

$$\dot{n}_B = -k_r^B \cdot n_B + k_2 \cdot n_E. \tag{A3}$$

In these expressions, k_r^A and k_r^B are the radiative decay rate constants of the higher- and lower-energy levels corresponding to the A and B emission bands, respectively, while E is the initial level reached in absorption/excitation. In this model the integrated rate expressions,[17] giving the time dependence of the population in the three excited levels E, A, and B, are

$$n_E(t) = n_0 \exp[-(k_1+k_2)\cdot t], \tag{A4}$$

$$n_A(t) = \frac{n_0 \cdot k_1}{k_1+k_2-k_r^A}\left[\exp(-k_r^A \cdot t) - \exp(-(k_1+k_2)\cdot t)\right], \tag{A5}$$

$$n_B(t) = \frac{n_0 \cdot k_2}{k_1+k_2-k_r^B}\left[\exp(-k_r^B \cdot t) - \exp(-(k_1+k_2)\cdot t)\right], \tag{A6}$$

where n_0 is the initial population in level E at time $t=0$, while the population of all other levels is zero at $t=0$. From inspection of expressions (A4)–(A6), giving the time dependence of population in the different levels, it can be stated that the rise times on the temporal profiles of the A and B emission bands, the terms having negative exponentials in Eqs. (A5) and (A6), will be identical, the reciprocal sum of k_1 and k_2, if such a relaxation mechanism exists. The different magnitudes of the rate constants k_1 and k_2 will therefore

not be manifested in the decay profiles of the A and B emissions, rather the ratios of the two rate constants determine the relative intensities of the two bands.

If an additional step, k_{22}, from a nonemitting intermediate level I is introduced in the relaxation leading to the population of the lower-energy level emission band B, as shown in the lower left of Fig. 12, then the time dependence of level B will then be given by

$$n_B(t)=n_0\cdot k_2\cdot k_{22}\,\frac{(k_1+k_2-k_{22})\exp(-k_r^B\cdot t)-(k_1+k_2-k_r^B)\exp(-k_{22}\cdot t)-(k_r^B-k_{22})\exp(-(k_1+k_2)\cdot t)}{(k_1+k_2-k_r^B)\cdot(k_{22}-k_1-k_2)\cdot(k_r^B-k_{22})}. \tag{A7}$$

The time dependence of the higher-energy emitting level A, will be unchanged from Eq. (A5), showing a rise time, $1/(k_1+k_2)$, which is too fast to be detected in the present measurements. In contrast, the time dependence in the B level is more complex exhibiting one decay and two rise components. In principle then three exponential functions would be required to fit such data. However, by comparing Eqs. (A7) and (A5) it can be stated that one of the rise times on the B level is identical to the very fast one not detectable on the upper A emission, while the second rise time is that extracted in the double exponential fits of the low-temperature decay curves. According to the model outlined above, the rate constant k_{22} is obtained directly as the reciprocal of the rate determining step resulting in the observed rise time on the B emission band. Above 11 K this step k_{22} is too fast to be detected with the temporal resolution (100 ps) of the present measurements.

2. High-temperature kinetics

The simplest kinetic scheme which could be presented to model the high-temperature behavior of the pair of Zn/Ar emission bands originating from an identical excitation is a four level scheme indicated on the bottom right of Fig. 12, having five decay paths. If it is assumed that relaxation steps k_1, k_2, and k_{22} leading to the populating of levels A and B are very fast compared to the nonradiative step $k_{\rm nr}$, interconnecting the emitting levels then the rate equations for levels A and B are

$$\dot{n}_A=-k_r^A\cdot n_A-k_{\rm nr}\cdot n_A+k_1\cdot n_E, \tag{A8}$$

$$\dot{n}_B=-k_r^B\cdot n_B+k_{\rm nr}\cdot n_A+k_2\cdot n_E. \tag{A9}$$

Integration of these rate equations yields the following expressions for the time dependence of the population in the emitting levels A and B:

$$n_A(t)=n_0\cdot k_1\,\frac{\exp[-(k_{\rm nr}+k_r^A)\cdot t]-\exp[-(k_1+k_2)\cdot t]}{k_1+k_2-k_{\rm nr}-k_r^A}, \tag{A10}$$

$$n_B(t)=n_0\cdot[X\,\exp(-k_r^B\cdot t)-Y\,\exp(-(k_{\rm nr}+k_r^A)\cdot t) - Z\,\exp(-(k_1+k_2)\cdot t)], \tag{A11}$$

where

$$X=\frac{k_1\cdot k_{\rm nr}+k_2\cdot k_{\rm nr}+k_2\cdot k_r^A-k_2\cdot k_r^B}{(k_1+k_2-k_r^B)\cdot(k_{\rm nr}+k_r^A-k_r^B)},$$

$$Y=\frac{k_1\cdot k_{\rm nr}}{(k_1+k_2-k_{\rm nr}-k_r^A)\cdot(k_{\rm nr}+k_r^A-k_r^B)},$$

and

$$Z=\frac{k_1\cdot k_2+k_2^2-k_2\cdot k_r^A-k_1\cdot k_{\rm nr}-k_2\cdot k_{\rm nr}}{(k_1+k_2-k_r^B)\cdot(k_1+k_2-k_{\rm nr}-k_r^A)}.$$

From inspection of the expressions for levels A and B, it can be stated that *the rise time on the B level* emission will be *identical* to the *observed decay time of level A* if a single relaxation step, of rate constant $k_{\rm nr}$ connects these two levels.

[1] V. A. Bracken, P. N. Kerins, P. Gürtler, and J. G. McCaffrey, J. Chem. Phys. **107**, 5290 (1997), preceding paper.

[2] B. Hoffmann-Millack, A. Klein, H. Lagier, B. Maid, and J. Hormes, Chem. Phys. **136**, 453 (1989).

[3] J. G. McCaffrey and P. N. Kerins, J. Chem. Phys. **106**, 7885 (1997).

[4] M. E. Fajardo, P. G. Carrick, and J. W. Kenney, J. Chem. Phys. **94**, 5812 (1991), and references cited therein.

[5] H. O. Wiggenhauser, W. Schröder, and D. M. Kolb, J. Chem. Phys. **88**, 3434 (1988).

[6] Deposition temperatures of 12, 18, and 25 K were used for the rare gases Ar, Kr, and Xe, respectively, while the maximum annealing temperatures of these solids were 33, 45, and 65 K.

[7] D. V. O'Connor and D. Phillips, *Time Correlated Single Photon Counting* (Academic, London, 1984).

[8] ZFIT program Nonlinear Least Squares Analysis of Fluorescence Decay Data by M. Rehorek, H. Otto, W. Rettig, A. Klock, and modified by P. Gürtler and M. Joppien, last update August 1995.

[9] The expressions and meanings of the lowest moments are as follows; the zeroth moment, $m_0=\int f(E)dE$ (area); first moment, $m_1=1/m_0\int Ef(E)dE$ (position) and the second moment, $m_2=1/m_0\int(E-m_1)^2f(E)dE$ (bandwidth), where $f(E)$ is the recorded spectral profile of the band.

[10] All the recorded decay profiles were fitted with double exponential functions with the exception of those recorded in the temperature range of 11–17 K inclusively, for which a single exponential sufficed. The major decay component of the fit contributed over 97% of the intensity.

[11] It was initially, but incorrectly, assumed that I_0 correlated to the intensity of the 218.9 nm decay at the lowest temperature recorded because of the temperature-dependent behavior displayed by the intensities of the emission bands in the low-temperature range of 9 to 13 K.

[12] D. Le Si Dang, R. Romestain, D. Simkin, and A. Fukuda, Phys. Rev. B **18**, 2989 (1978).

[13] M. Casalboni, F. Crisanti, U. M. Grassano, C. Manfroncelli, A. Scacco, and A. Tanga, Phys. Status Solidi (B) **93**, 755 (1979).

[14] Time-resolved measurements of the near-uv emissions could not be recorded as the repetition rate of the storage ring was too high, even for ''single-bunch'' mode operation with a repetition rate of 1.042 MHz. With

a repetition rate of 1.042 MHz, the decay time of the near-uv emissions must therefore be longer than 10 μs.
[15] V. A. Bracken, Ph.D. thesis, National University of Ireland, Maynooth, 1997.
[16] J. G. McCaffrey and P. N. Kerins (unpublished).
[17] These integrations are most easily accomplished using the operational calculus of a Laplace transform. For a description of the method, see, J. I. Steinfeld, J. S. Francisco, and W. L. Hase, *Chemical Kinetics and Dynamics* (Prentice-Hall, Englewood Cliffs, NJ, 1991); and for tables of the required inverse Laplace transforms see, A. Erdelyi, W. Magnus, F. Oberhettinger, and F. Tricomi, *Tables of Integral Transform* (McGraw-Hill, New York, 1954), Vols. 1 and 2.